ELSEVIER

Earth and Planetary Science Letters 201 (2002) 575–591

EPSL

www.elsevier.com/locate/epsl

^{21}Ne versus ^{10}Be and ^{26}Al exposure ages of fluvial terraces: the influence of crustal Ne in quartz

Ralf Hetzel [a,b,*], Samuel Niedermann [a], Susan Ivy-Ochs [c], Peter W. Kubik [d], Mingxin Tao [e], Bo Gao [e]

[a] *GeoForschungsZentrum Potsdam, Telegrafenberg, 14473 Potsdam, Germany*
[b] *Institut für Geowissenschaften, Universität Potsdam, 14415 Potsdam, Germany*
[c] *Institute of Particle Physics, ETH Hönggerberg, 8093 Zurich, Switzerland*
[d] *Paul Scherrer Institut, c/o Institute of Particle Physics, ETH Hönggerberg, 8093 Zurich, Switzerland*
[e] *The State Key Laboratory of Gas-geochemistry, Lanzhou Institute of Geology, Chinese Academy of Science, 324 Donggang West Avenue, Lanzhou 730000, PR China*

Received 7 January 2002; received in revised form 29 May 2002; accepted 31 May 2002

Abstract

The accuracy of ^{21}Ne surface exposure ages depends critically on the correction for a trapped Ne component. Commonly, the amount of cosmogenic Ne used to calculate ^{21}Ne exposure ages is considered to be the Ne excess relative to a trapped component of atmospheric composition (^{21}Ne/^{20}Ne = 0.00296). Here, we document a trapped Ne component in quartz samples from a series of river terraces at the northern margin of Tibet [Hetzel et al., Nature 417 (2002) 428–432], which has a non-atmospheric ^{21}Ne/^{20}Ne ratio varying from 0.00299 to 0.00398. Vacuum crushing of amalgamated samples, each derived from 30–80 quartz clasts, revealed that the non-atmospheric trapped component is present in fluid inclusions. It has probably been incorporated into the quartz crystals during their growth in veins at low-grade metamorphic conditions. Only if the amount of cosmogenic ^{21}Ne is determined relative to this trapped component are the calculated ^{21}Ne exposure ages consistent with the relative ages of the tectonically induced terraces and in agreement with independent ^{10}Be and ^{26}Al exposure ages of the fluvial terraces. A significant in situ production of nucleogenic ^{21}Ne by the reaction ^{18}O(α,n)^{21}Ne in the Paleozoic quartz minerals is ruled out by extremely low U contents of the order of 1–5 ppb. All ages have been corrected for an inherited cosmogenic component that results from cosmic ray exposure during erosion of the host rock and transport of the clasts to the terraces. The origin of the trapped component from crustal fluids is supported by high ^{40}Ar/^{36}Ar ratios of 2000–6000 and slightly elevated ^{136}Xe/^{132}Xe ratios relative to air, which can be explained by radioactive decay of ^{40}K and spontaneous fission of U in the crust.

Keywords: Ne-21; cosmogenic elements; quartz; exposure age; terraces

1. Introduction

^{21}Ne and ^{10}Be are among the cosmogenic nuclides most widely used for surface exposure dating. While both ^{21}Ne and ^{10}Be are produced by

* Corresponding author. Tel.: +49-331-288-1423.
E-mail address: hetzel@gfz-potsdam.de (R. Hetzel).

0012-821X/02/$ – see front matter
PII: S0012-821X(02)00748-3

cosmic rays in silicates, there is a fundamental difference between them: ^{10}Be is radioactive and has a half-life of 1.5 Ma, whereas ^{21}Ne is stable. As a consequence, non-cosmogenic ^{10}Be usually does not accumulate to significant amounts over geological time, because due to its radioactive decay it reaches a saturation level that is orders of magnitude lower than typical concentrations of cosmogenic ^{10}Be [1]. A similar case can be made for ^{26}Al, another radionuclide with a half-life of 0.7 Ma, although rocks with a high Na content may contain appreciable amounts of nucleogenic ^{26}Al from the ^{23}Na(α,n)^{26}Al reaction [1]. In contrast, processes that lead to the production or incorporation of non-cosmogenic ^{21}Ne in the mineral to be dated must be carefully evaluated in order to derive geologically meaningful exposure ages.

Despite the problems associated with the potential presence of non-cosmogenic noble gas components, stable nuclides such as ^{21}Ne offer a number of advantages compared to radionuclides. ^{21}Ne allows one to investigate exposure histories which are longer than the limit of a few million years imposed by the half-life of ^{10}Be, the longest-lived radionuclide commonly used. It is even possible to study 'paleo-exposures' [2], i.e. surface exposures which occurred many million years ago in rock which was later covered permanently. In addition, the typical sample size needed for noble gas studies is much smaller than for radionuclide analyses. Whereas 0.5–1 g of quartz is usually sufficient to determine cosmogenic ^{21}Ne concentrations, some 20–30 g of quartz are required to achieve a similar accuracy for ^{10}Be and ^{26}Al. For many applications a combined study of cosmogenic noble gases and radionuclides will be useful, for example in order to identify and evaluate complex exposure histories. Therefore, even though radionuclide data may often be easier to interpret, it is essential to further develop the Ne technique as well, which is one of the purposes of the present investigation.

The different Ne components which may be contained in a mineral or rock are best visualized in a neon three-isotope diagram (Fig. 1). As cosmic ray-produced Ne (Ne_c) is characterized by a unique ^{22}Ne/^{21}Ne ratio, mixtures of cosmogenic

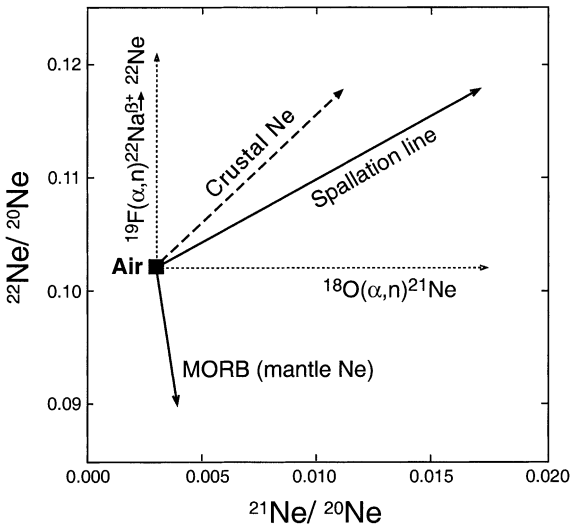

Fig. 1. Ne three-isotope diagram (^{22}Ne/^{20}Ne versus ^{21}Ne/^{20}Ne) showing the compositions and mixing trends of various Ne components. Isotopic ratios for air are ^{21}Ne/^{20}Ne = 0.002959 and ^{22}Ne/^{20}Ne = 0.1020 [3]. Mixtures of cosmogenic and atmospheric neon plot on the 'spallation line' [4]. Contributions from nucleogenic ^{21}Ne and ^{22}Ne are characterized by shifts in horizontal and vertical directions, respectively. Trend lines for crustal Ne [5] and MORB-type Ne [6] are also given.

and atmospheric Ne must plot on the 'spallation line'. The slope of the spallation line is experimentally well determined to lie between 1.10 and 1.14, corresponding to a ^{22}Ne/^{21}Ne production ratio between 1.20 and 1.27 for the mineral quartz [4,7–9]. Apart from atmospheric Ne, a number of other non-cosmogenic Ne components may be present in a rock. Magmatic or metamorphic fluids in the crust or mantle may contain significant amounts of Ne. Crustal Ne, as determined in methane-rich natural gases [5], has somewhat higher ^{22}Ne/^{21}Ne ratios than Ne_c (Fig. 1). However, the ^{22}Ne/^{21}Ne ratio may vary with source rock composition and may not always be distinguished from Ne_c. If Ne from fluids is incorporated into a rock during growth or recrystallization of its mineral constituents, it is referred to as trapped Ne (Ne_{tr}). Nucleogenic Ne (Ne_n) is produced by interaction of α-particles and neutrons from the radioactive decay of U and Th with neighboring nuclei such as ^{18}O, ^{19}F, ^{24}Mg and ^{25}Mg [10]. Due to the 10–30 μm range of

α-particles Ne_n is either produced within the minerals containing U and Th or in adjacent mineral grains into which the α-particles are injected [11,12]. Examples of reactions producing Ne_n are $^{18}O(\alpha,n)^{21}Ne$, $^{19}F(\alpha,n)^{22}Na(\beta^+)^{22}Ne$ and $^{24,25}Mg(n,\alpha)^{21,22}Ne$.

The mineral most widely used in surface exposure dating is quartz. As concentrations of F and Mg in quartz are negligible, the only reaction that may produce significant amounts of Ne_n within the crystal lattice of quartz is the reaction $^{18}O(\alpha,n)^{21}Ne$. Even low concentrations of U and Th may lead to the in situ production of significant amounts of $^{21}Ne_n$ in old rocks. On the other hand, Ne_{tr} may be incorporated during growth or recrystallization of the quartz from a fluid phase [13]. Thus, the commonly used assumption that Ne_{tr} is atmospheric in composition might generally not be correct. While for samples with a surface exposure age of several million years (e.g. [7,9,14]) small amounts of non-cosmogenic Ne may be insignificant, the need to quantify the contribution of non-cosmogenic Ne increases as exposure ages decrease. In this study, we demonstrate that for quartz samples with ages on the order of 10^4–10^5 yr, the presence of a crustal Ne component with a non-atmospheric composition must be evaluated and corrected for, in order to derive geologically meaningful ^{21}Ne exposure ages. The geological implications of these surface exposure ages for the active tectonics and landscape evolution at the northern margin of Tibet are discussed in a separate contribution [15].

2. Geological setting and description of the terraces

The studied terraces are located at the mountain front of the Qilian Shan, an active fold-and-thrust belt that extends for about 600 km along the northeastern margin of the Tibetan plateau [16]. The Qilian Shan mountain front is defined by active thrust faults and huge alluvial fans extending into the Hexi corridor (Fig. 2). Active crustal shortening in the Qilian Shan propagates north-northeast and therefore new thrust faults displace the alluvial fan deposits. When such thrusts become active, sedimentation on the coalesced alluvial fan surfaces stops due to hanging wall uplift and rivers crossing the active faults will downcut and form river terraces [15].

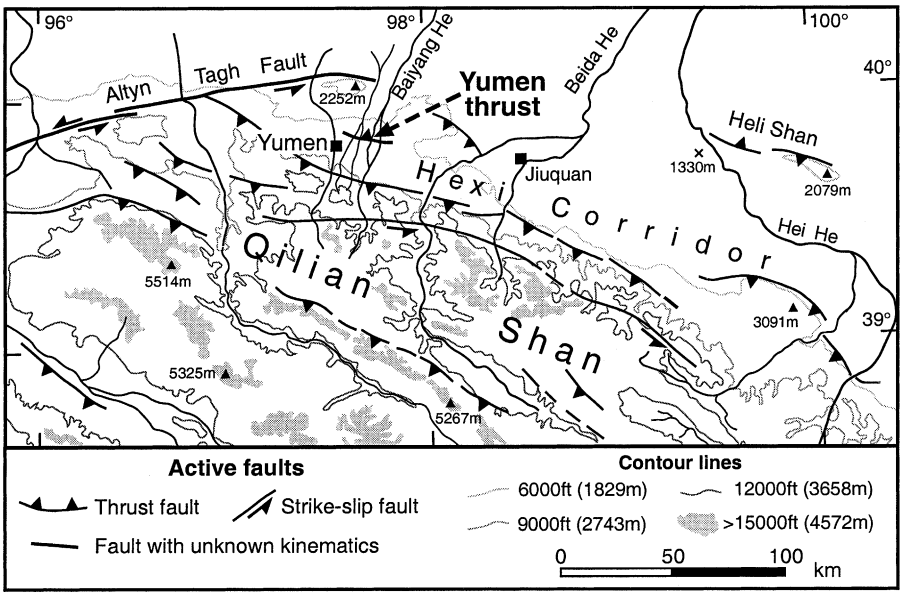

Fig. 2. Morphotectonic map of the northwestern Qilian Shan showing the location of the Yumen thrust. The investigated terraces at the Yumen thrust have formed adjacent to the thrust fault due to hanging wall uplift. For a detailed location map see [15].

A spectacular example of such a young thrust fault occurs northeast of Yumen, ~10 km north of the steep Qilian Shan mountain front at an elevation of 2000 m (Fig. 2). This north-dipping Yumen thrust forms a 25 km long south-facing fault scarp. North-flowing rivers draining the Qilian Shan have incised into the uplifting hanging wall and formed a large number of river terraces. The Baiyang He (Chinese: 'He' = river) is the largest of these intermittent streams that cross the Yumen thrust. It extends 60 km to the south and its catchment area in the Qilian Shan reaches elevations up to 5000 m (Fig. 2). The catchment of streams that transect the western part of the Yumen thrust is much smaller and reaches an elevation of only about 4000 m. Lithologies exposed in these catchments are dominated by Early Paleozoic low-grade metamorphic sediments and minor amounts of Precambrian crystalline basement and granite.

The present study concentrates on six different terrace levels at two sites in the western and central portion of the Yumen thrust. The elevation of the different terraces above active river channels largely reflects the amount of tectonic uplift and has been quantified by a detailed topographic survey [15]. The highest terrace level is located at site 1 in the central part of the thrust, 57 m above an active channel of the Baiyang He. At site 2 in the western portion of the thrust, a series of six terraces at elevations between 43 and 4 m above an active river channel is present [15] (see figure A1 of the **Background Data Set**[1] for a photograph of the terraces at site 2). The lowermost terrace has not been sampled for exposure dating. The elongated terraces at site 2 are 30–80 m wide and separated by north–south trending erosional channels a few meters deep. Due to arid climate conditions with annual precipitation on the order of 200–300 mm, there is no vegetation on the terraces. Pristine parts of individual terraces are separated by erosional rills not deeper than a few decimeters.

Clasts on the terrace surfaces are rounded and most of them are 0.5–5 cm in size. Clasts are dominated by quartzite, phyllite and carbonate, whereas volcanic, gneiss and granite clasts are rare. The individual clasts are in contact with each other and minor amounts of sand are restricted to the interstitial space between the clasts. Sand grains and clasts are cemented by carbonate and gypsum, which are present in the uppermost centimeters of the terrace deposits. Many of the foliated phyllite and gneiss clasts have suffered an in situ fragmentation along the schistosity, with the angular fragments still being close to each other. Carbonate clasts show dissolution features on their surfaces. Most clasts have films of brown desert varnish, although quartz clasts commonly do not show these coatings. During two field trips in September 1999 and 2000 we observed that even strong winds were not able to remove any dust particles from the terraces, whereas large dust clouds could be seen above the active alluvial fans along the Qilian Shan mountain front. Taken together, these observations demonstrate that the terrace surfaces are stable geomorphic features.

3. Sampling strategy

When dating depositional surfaces such as river terraces or alluvial fans it is important to take into account that cosmogenic nuclides are not only generated after a clast has been deposited but are already produced during erosion of the host rock and transport of the clast on slopes and in rivers. For each clast, this pre-depositional inherited component is different and only a mean value from amalgamated samples consisting of many clasts [17] will yield geologically meaningful information. Numerical modeling using plausible transport and exhumation scenarios suggests that 30 clasts are sufficient to constrain the mean inheritance of cosmogenic nuclides to ±20% [18,19]. In principle, there are two ways to determine the inherited nuclide component, which has also been referred to as 'geological blank' [20]. The first way is to analyze amalgamated samples from presently active river channels and assume that the erosion and transport rates of these clasts are similar to those in the past, when the terraces to be dated were formed. Second, the inherited

[1] http://www.elsevier.com/locate/epsl

component can be extracted from subsurface samples, if no post-depositional displacement of the clasts within the deposit has occurred and the transport and depositional processes were invariant in the sedimentary sequence. If the latter assumptions are correct, the concentration of cosmogenic nuclides should show an exponential decrease with depth, and a concentration versus depth plot should asymptotically approach the mean inheritance at depth [18,19].

We collected 100–300 quartz clasts from the most pristine-looking part of the six terraces at the Yumen thrust within circles of 5–10 m in diameter. The relief within the sampled area on all terraces was determined to be in the range of 3 cm to at most 10 cm using a string fixed in the center of the circle. The small relief of the terraces suggests that the mean amount of erosional denudation is only on the order of a few centimeters. Sampling for exposure dating has concentrated on quartzite clasts for the following reasons. Granite and gneiss clasts on the terraces are rare and it is not possible to collect a sufficient number of clasts to apply the amalgamation approach outlined above. On the other hand, abundant phyllite clasts have not been sampled because: (i) the separation of quartz from this fine-grained rock type is difficult and (ii) phyllites may have high concentrations of U and Th and thus may contain considerable amounts of Ne_n. The quartz clasts on all terraces have a milky gray to white color, due to the presence of abundant fluid inclusions, and are most likely derived from quartz veins, which have been observed in the low-grade metamorphic Paleozoic sediments in the Qilian Shan source area. Quartz veins typically form in metapelites during prograde greenschist-facies metamorphic reactions that deliberate SiO_2.

In order to constrain the concentration of inherited cosmogenic nuclides, we have taken two amalgamated quartz samples from active river channels, one sample in the central part of the thrust from an active river bed 800 m west-northwest of site 1 and one sample from the active river that formed the terraces at site 2. In addition, we took three subsurface quartz samples at 0.6–0.65, 1.2–1.25 and 1.8–1.85 m depth from a hole excavated on the uplifted alluvial fan surface at site 2. The sediments exposed in a 1.8×1.3 m wide hole on terrace T_1 neither showed any signs of bioturbation nor evidence for soil formation, except thin films of carbonate around some clasts. No organic material is present in the sediments. The hole revealed that the alluvial fan sediments beneath the surface consist of 50–90% sand, i.e. the amount of clasts is much lower than on the surface. We interpret the high concentrations of clasts on the terrace surfaces to result from the rapid deflation of silt- and sand-sized particles and a relative enrichment of larger clasts. Once a critical concentration of clasts has been attained on the surface, deflation becomes ineffective and eventually stops and the terrace is a stable geomorphic surface.

4. Preparation of quartz separates and analytical procedures

From the 100–300 quartz clasts that were collected for each sample in the field, 30–80 clasts were selected on the basis that milky gray colored clasts have probably less fluid inclusions than white clasts. The selected quartz clasts, which had a similar size of commonly 2–3 cm, were crushed with a steel mortar and sieved in three size fractions. From the first samples (99C8, 99C12), the 500–1000 μm fraction was used for further chemical treatment, while for all subsequent samples a smaller size fraction of 250–500 μm was chosen. Conventional magnetic separation techniques did not improve the quality of these size fractions. The chemical treatment of the samples involved a first leaching in HCl at a temperature of ~80°C for 4–5 h, followed by a series of three leachings, each between 5 and 10 h, in a dilute HF/HNO_3 mixture at 80°C in an ultrasonic bath. The etching in the HF/HNO_3 mixture removed at least several micrometers of the surfaces of the quartz grains and eliminated meteoric ^{10}Be. Furthermore, the contribution of $^{21}Ne_n$ which could have been produced from $^{18}O(\alpha,n)$ in the surface layer due to injection of α-particles from neighboring minerals would also be reduced by the etching. The details of the chemical isolation procedure have been described in [21]. Al concentrations in four quartz separates also used for ^{26}Al

Table 1
Ne, Ar and Xe data of quartz from terraces at the Yumen thrust, Qilian Shan, China

Locality Sample ID	Grain size (μm)	T (°C)	^{20}Ne ($\times10^{-12}$ cl/g)	^{22}Ne/^{20}Ne ($\times10^{-2}$)	^{21}Ne/^{20}Ne ($\times10^{-3}$)	^{21}Ne[b] ($\times10^{6}$ atoms/g)	Error	^{21}Ne[c] ($\times10^{6}$ atoms/g)	Error	^{40}Ar ($\times10^{-8}$ cm^3/g)	^{40}Ar/^{36}Ar	^{132}Xe ($\times10^{-12}$ cm^3/g)	^{134}Xe/^{132}Xe	^{136}Xe/^{132}Xe
Site 1: terrace, 57 m		400	117.0 ± 6.0	10.502 ± 0.086	5.95 ± 0.21	9.41	± 0.82	7.79	± 0.81	17.59 ± 0.88	528.1 ± 3.0	1.73 ± 0.11	–	–
		600	374 ± 19	10.266 ± 0.056	4.20 ± 0.14	12.5	± 1.5	7.3	± 1.6	25.5 ± 1.3	1120.5 ± 8.4	2.10 ± 0.12	–	–
		800	304 ± 15	10.293 ± 0.079	3.646 ± 0.080	5.60	± 0.71	1.41	± 0.87	12.88 ± 0.65	1845 ± 46	2.75 ± 0.15	0.391 ± 0.011	0.3314 ± 0.0058
		1700	10.9 ± 1.0	10.95 ± 0.79	3.58 ± 0.43	–	–	–	–	270 ± 18	4005 ± 42	20.2 ± 1.0	0.3915 ± 0.0038	0.3323 ± 0.0032
99C12	< 100	total	806 ± 25	10.319 ± 0.043	4.236 ± 0.080	27.5	± 1.9	16.5	± 2.0	326 ± 18	2499 ± 63	26.8 ± 1.0	–	–
	500–1000	crush	187.8 ± 9.6	10.237 ± 0.088	3.473 ± 0.070	–	–	–	–	59.7 ± 4.0	2876 ± 26	1.768 ± 0.090	0.4011 ± 0.0061	0.349 ± 0.013
Active river, 800 m WNW of site 2		400	142.0 ± 7.3	10.07 ± 0.11	2.998 ± 0.061	0.15	± 0.23	0.0	± 0.0	9.08 ± 0.46	539.3 ± 5.6	0.276 ± 042	–	–
		600	695 ± 36	10.142 ± 0.053	3.305 ± 0.051	6.5	± 1.0	2.2	± 1.7	96 ± 11	1553 ± 16	1.79 ± 0.36	–	–
		800	909 ± 50	10.170 ± 0.057	3.287 ± 0.054	8.0	± 1.4	2.4	± 2.3	24.8 ± 1.2	3647 ± 76	0.662 ± 0.080	0.403 ± 0.014	0.344 ± 0.013
		1700	114.1 ± 6.0	10.40 ± 0.15	3.39 ± 0.17	–	–	–	–	520 ± 96	6060 ± 120	6.02 ± 0.32	0.4001 ± 0.0064	0.3451 ± 0.0078
99C13	250–500	total	1860 ± 62	10.166 ± 0.036	3.277 ± 0.034	14.6	± 1.7	4.6	± 2.8	650 ± 97	3790 ± 240	8.75 ± 0.49	–	–
	250–500	crush	185.7 ± 9.5	10.178 ± 0.089	3.189 ± 0.075	–	–	–	–	56.5 ± 3.9	2933 ± 35	0.964 ± 0.050	0.4067 ± 0.0058	0.3527 ± 0.0099
Site 2: T_1, 43 m		400	130.7 ± 6.7	10.29 ± 0.11	4.84 ± 0.14	6.59	± 0.59	6.29	± 0.62	13.06 ± 0.66	545.0 ± 4.4	2.28 ± 0.19	–	–
		600	410 ± 21	10.165 ± 0.086	3.321 ± 0.097	3.99	± 1.1	3.04	± 1.3	20.7 ± 1.0	1061.4 ± 9.2	2.82 ± 0.24	–	–
		800	247 ± 13	10.208 ± 0.074	3.11 ± 0.12	1.00	± 0.78	0.43	+0.87/−0.43	7.87 ± 0.41	1226 ± 32	3.23 ± 0.27	0.3876 ± 0.0089	0.3273 ± 0.0083
		1700	10.1 ± 1.0	11.14 ± 0.72	3.51 ± 0.58	–	–	–	–	225 ± 15	3702 ± 38	21.3 ± 1.7	0.3891 ± 0.0040	0.3293 ± 0.0029
99C8	< 100	total	798 ± 26	10.211 ± 0.053	3.507 ± 0.068	11.6	± 1.5	9.8	+1.7/−1.5	267 ± 15	2409 ± 57	29.6 ± 1.7	–	–
	500–1000	crush	131.1 ± 6.7	10.187 ± 0.056[a]	3.045 ± 0.060[a]	–	–	–	–	25.5 ± 1.3	2191 ± 43	0.597 ± 0.034	0.406 ± 0.011	0.357 ± 0.018
Site 2: T_{2a}, 38 m		400	74.4 ± 3.9	10.71 ± 0.17	7.49 ± 0.33	9.07	± 0.81	7.04	± 0.79	23.6 ± 1.2	338.8 ± 1.2	10.84 ± 0.65	–	–
		600	267 ± 14	10.36 ± 0.11	4.46 ± 0.10	10.77	± 0.89	3.48	± 1.0	32.4 ± 1.6	401.6 ± 1.6	12.19 ± 0.74	–	–
		800	74.4 ± 4.0	10.36 ± 0.15	4.05 ± 0.26	2.19	± 0.52	0.16	± 0.038	12.29 ± 0.63	813 ± 11	10.06 ± 0.61	0.3860 ± 0.0038	0.3260 ± 0.0031
		1700	3.59 ± 0.73	10.21 ± 0.69	4.73 ± 0.95	–	–	–	–	76.1 ± 7.8	3130 ± 180	50.4 ± 3.0	0.3873 ± 0.0024	0.3277 ± 0.0023
99C10	< 50	total	419 ± 15	10.422 ± 0.079	4.93 ± 0.10	22.0	± 1.3	10.7	± 1.3	144.4 ± 8.1	761 ± 40	83.5 ± 3.2	–	–
	250–500	crush	191.4 ± 9.9	10.322 ± 0.074	3.975 ± 0.096	–	–	–	–	47.2 ± 3.3	2865 ± 35	0.707 ± 0.039	0.413 ± 0.016	0.361 ± 0.014
Site 2: T_{2b}, 35 m		400	148.2 ± 7.8	10.428 ± 0.065	5.14 ± 0.12	8.68	± 0.64	7.20	± 0.69	25.5 ± 1.3	366.2 ± 3.2	3.83 ± 0.23	0.3892 ± 0.0045	0.3333 ± 0.0075
		600	200 ± 10	10.222 ± 0.059	3.30 ± 0.11	1.83	± 0.60	0.0	+0.58/−0.0	15.75 ± 0.81	494.6 ± 3.3	2.25 ± 0.12	0.3923 ± 0.0073	0.3322 ± 0.0081
		800	39.1 ± 2.5	10.37 ± 0.19	3.12 ± 0.29	0.17	+0.3/−0.17	0.0	+0.10/−0.0	4.77 ± 0.27	612 ± 15	3.12 ± 0.16	0.3882 ± 0.0079	0.3285 ± 0.0047
		1750[d]	–	–	–	–	–	–	–	81.9 ± 5.7	3980 ± 170	19.35 ± 0.98	0.3877 ± 0.0037	0.3290 ± 0.0035
00C13	< 50	total	387 ± 13	10.315 ± 0.044	3.986 ± 0.084	10.68	+0.93/−0.89	7.20	+0.90/−0.69	127.9 ± 5.9	985 ± 46	28.6 ± 1.0	0.3883 ± 0.0028	0.3298 ± 0.0027
	250–500	crush	69.4 ± 3.1[a]	10.202 ± 0.048[a]	3.330 ± 0.083[a]	–	–	–	–	27.0 ± 1.4	3960 ± 100	0.620 ± 0.062	0.409 ± 0.022	0.359 ± 0.017
Site 2: T_3, 21 m		400	51.5 ± 2.7	10.32 ± 0.16	5.34 ± 0.29	3.30	± 0.44	3.05	± 0.45	7.44 ± 0.37	382.1 ± 4.2	0.827 ± 0.051	–	–
		600	216 ± 11	10.20 ± 0.11	3.76 ± 0.16	4.61	± 0.96	3.6	± 1.1	18.54 ± 0.93	556.7 ± 5.2	1.607 ± 0.089	–	–
		800	208 ± 11	10.21 ± 0.13	3.19 ± 0.13	1.30	± 0.73	0.30	+0.9/−0.30	9.25 ± 0.48	945 ± 17	1.494 ± 0.087	0.387 ± 0.013	0.3278 ± 0.0087
		1700	6.67 ± 0.91	10.67 ± 0.45	3.30 ± 0.47	–	–	–	–	88.3 ± 9.2	2731 ± 75	7.84 ± 0.42	0.3888 ± 0.0054	0.3306 ± 0.0054
99C11	< 50	total	482 ± 16	10.222 ± 0.076	3.676 ± 0.097	9.2	± 1.3	6.9	+1.5/−1.2	123.5 ± 9.3	1302 ± 59	11.77 ± 0.44	–	–
	250–500	crush	55.2 ± 3.0[a]	10.172 ± 0.052[a]	3.138 ± 0.095[a]	–	–	–	–	17.1 ± 1.4	2358 ± 32	0.338 ± 0.033	0.415 ± 0.015	0.357 ± 0.015

Table 1 (*Continued*).

Locality Sample ID	Grain size (μm)	T (°C)	^{20}Ne ($\times10^{-12}$ cl/g)	$^{22}Ne/^{20}Ne$ ($\times10^{-2}$)	$^{21}Ne/^{20}Ne$ ($\times10^{-3}$)	$^{21}Ne^{b}$ ($\times10^{6}$ atoms/g)	Error	$^{21}Ne^{c}$ ($\times10^{6}$ atoms/g)	Error	^{40}Ar ($\times10^{-8}$ cm^3/g)	$^{40}Ar/^{36}Ar$	^{132}Xe ($\times10^{-12}$ cm^3/g)	$^{134}Xe/^{132}Xe$	$^{136}Xe/^{132}Xe$
Site 2: T_4, 18 m		400	47.2 ± 2.7	10.125 ± 0.089	3.63 ± 0.26	0.84	± 0.33	0.57	± 0.34	4.97 ± 0.51	434.1 ± 5.3	1.74 ± 0.37	0.3907 ± 0.0088	0.3288 ± 0.0051
		600	166.2 ± 8.6	10.237 ± 0.073	3.806 ± 0.055	3.78	± 0.31	2.81	± 0.46	29.7 ± 1.5	708.0 ± 4.2	2.27 ± 0.13	0.3924 ± 0.0082	0.333 ± 0.010
		800	424 ± 23	10.182 ± 0.088	3.270 ± 0.070	3.54	± 0.82	1.1	+1.2/−1.1	29.3 ± 1.5	1660 ± 24	2.00 ± 0.12	0.3964 ± 0.0058	0.339 ± 0.011
		1700[d]	–	–	–	–	–	–	–	154 ± 11	3515 ± 77	13.00 ± 0.66	0.3901 ± 0.0044	0.3330 ± 0.0049
00C10	< 50	total	637 ± 25	10.192 ± 0.062	3.436 ± 0.053	8.16	0.94	4.5	+1.4/−1.2	218 ± 11	1898 ± 59	19.01 ± 0.78	0.3911 ± 0.0033	0.3332 ± 0.0038
	250–500	crush	113.8 ± 5.9	10.181 ± 0.073	3.176 ± 0.081	–	–	–	–	38.5 ± 2.6	3733 ± 85	0.846 ± 0.043	0.4037 ± 0.0090	0.357 ± 0.017
Site 2: active river		400	42.1 ± 2.2	10.04 ± 0.21	3.19 ± 0.19	0.26	± 0.22	0.18	+0.23/−0.18	9.08 ± 0.46	584.0 ± 6.2	0.377 ± 0.041	–	–
		600	441 ± 25	10.179 ± 0.086	3.14 ± 0.13	2.1	± 1.5	1.2	+1.8/−1.2	40.6 ± 2.0	2098 ± 30	0.698 ± 0.084	–	–
		800	430 ± 22	10.159 ± 0.061	3.007 ± 0.083	0.6	+1.0/−0.6	0.0	+0.94/−0.0	5.00 ± 0.26	2340 ± 120	0.144 ± 0.030	0.389 ± 0.018	0.340 ± 0.016
		1700	72.2 ± 3.8	10.33 ± 0.13	3.06 ± 0.11	–	–	–	–	183 ± 19	2275 ± 28	2.67 ± 0.19	0.4098 ± 0.0052	0.3561 ± 0.0048
99C9	250–500	total	985 ± 34	10.175 ± 0.049	3.078 ± 0.069	3.0	+1.8/−1.6	1.4	+2.0/−1.2	238 ± 19	2023 ± 28	3.89 ± 0.21	–	–
	250–500	crush	144.8 ± 7.9	10.187 ± 0.047	3.037 ± 0.075	–	–	–	–	24.4 ± 1.2	2040 ± 40	0.402 ± 0.031	0.423 ± 0.015	0.372 ± 0.016
Site 2: subsurface, 0.6–0.65 m on T_1		400	343 ± 18	10.215 ± 0.053	3.573 ± 0.089	5.66	± 0.87	4.3	± 1.1	33.5 ± 1.7	367.7 ± 1.4	5.00 ± 0.28	0.3916 ± 0.0043	0.3314 ± 0.0049
		600	448 ± 23	10.196 ± 0.060	3.132 ± 0.051	2.08	± 0.62	0.30	+01.1/−0.30	18.05 ± 0.92	767.3 ± 9.0	3.69 ± 0.19	0.3919 ± 0.0068	0.3323 ± 0.0063
		800	36.5 ± 2.3	10.34 ± 0.16	3.11 ± 0.25	0.15	+0.25/−0.15	0.0	+0.26/−0.0	3.67 ± 0.21	897 ± 44	4.12 ± 0.21	0.3888 ± 0.0087	0.3263 ± 0.0057
		1750[d]	–	–	–	–	–	–	–	223 ± 15	3977 ± 51	18.54 ± 0.94	0.3912 ± 0.0037	0.3354 ± 0.0077
00C11A	< 50	total	828 ± 29	10.210 ± 0.040	3.314 ± 0.048	7.9	± 1.1	4.6	+1.6/−1.1	278 ± 15	1592 ± 63	31.4 ± 1.0	0.3910 ± 0.0027	0.3332 ± 0.0047
	250–500	crush	53.3 ± 2.3[a]	10.159 ± 0.085[a]	3.107 ± 0.077[a]	–	–	–	–	15.16 ± 0.77	2192 ± 60	0.403 ± 0.030	0.407 ± 0.015	0.353 ± 0.020
Site 2: subsurface, 1.2–1.25 m on T_1		400	295 ± 15	10.210 ± 0.099	3.38 ± 0.15	3.4	± 1.2	2.3	± 1.3	33.5 ± 1.7	350.5 ± 1.6	5.04 ± 0.28	0.3908 ± 0.0092	0.3325 ± 0.0097
		600	331 ± 17	10.291 ± 0.046	3.135 ± 0.075	1.56	± 0.67	0.39	+0.83/−0.39	17.9 ± 1.0	531.9 ± 8.1	[e]	[e]	[e]
		800	21.6 ± 1.7	10.43 ± 0.26	3.20 ± 0.24	0.14	± 0.14	0.06	+0.14/−0.06	3.86 ± 0.22	583 ± 15	4.75 ± 0.25	0.3883 ± 0.0086	0.3287 ± 0.0035
		1750[d]	–	–	–	–	–	–	–	115.5 ± 8.0	2429 ± 46	19.15 ± 0.97	0.3903 ± 0.0039	0.3320 ± 0.0069
00C11B	< 50	total	647 ± 23	10.259 ± 0.052	3.250 ± 0.079	5.1	± 1.4	2.8	+1.5/−1.3	170.8 ± 8.2	931 ± 33	–	–	–
	250–500	crush	70.8 ± 4.9	10.129 ± 0.097	3.091 ± 0.056	–	–	–	–	15.28 ± 0.77	1864 ± 36	0.211 ± 0.020	0.411 ± 0.029	0.359 ± 0.019
Site 2: subsurface, 1.8–1.85 m on T_1		400	423 ± 22	10.149 ± 0.068	3.179 ± 0.088	2.5	± 1.0	2.1	± 1.3	39.5 ± 2.0	393.2 ± 1.5	3.72 ± 0.23	0.3941 ± 0.0074	0.3367 ± 0.0086
		600	543 ± 28	10.177 ± 0.077	3.047 ± 0.055	1.28	± 0.81	0.78	+1.4/−0.78	22.7 ± 1.2	1008 ± 14	2.24 ± 0.13	0.3925 ± 0.0073	0.3376 ± 0.0082
		800	56.2 ± 3.2	10.30 ± 0.14	3.10 ± 0.23	0.21	+0.34/−0.21	0.15	+0.36/−0.15	3.46 ± 0.20	939 ± 52	3.05 ± 0.16	0.3865 ± 0.0051	0.3251 ± 0.0055
		1750[d]	–	–	–	–	–	–	–	242 ± 17	3888 ± 64	12.84 ± 0.65	0.3935 ± 0.0043	0.338 ± 0.010
00C11C	< 50	total	1022 ± 36	10.172 ± 0.050	3.104 ± 0.049	4.0	± 1.3	3.1	+1.9/−1.5	308 ± 17	1629 ± 66	21.85 ± 0.72	0.3925 ± 0.0030	0.3359 ± 0.0062
	250–500	crush	127.8 ± 5.3[a]	10.106 ± 0.053[a]	2.993 ± 0.075[a]	–	–	–	–	20.4 ± 1.0	1532 ± 18	0.366 ± 0.033	0.409 ± 0.020	0.352 ± 0.015

All errors are 2σ.

[a] Mean of two measurements.

[b] Excess ^{21}Ne calculated relative to $^{21}Ne/^{20}Ne$ of air (^{21}Ne released at 1700°C is neglected).

[c] Excess ^{21}Ne relative to $^{21}Ne/^{20}Ne$ of trapped component released by crush (^{21}Ne released at 1700°C is neglected).

[d] Unreliable Ne data due to neon degassing from crucible (see text).

[e] Gas fraction was lost due to manual operation error.

exposure dating were only 25–30 ppm, indicating that the procedure had effectively removed all meteoric ^{10}Be [21].

Noble gas analysis of the quartz separates was carried out in the noble gas laboratory of the GFZ Potsdam. Gas extraction was accomplished by both stepwise heating and mechanical crushing of aliquots. Sample weights were 0.6–0.9 g for step-heated samples and 1–1.5 g for crushed samples. For crushing, the quartz obtained from the chemical isolation procedure was used without further treatment. Thus, the grain size of these aliquots is similar to that of the sieved size fraction. With the exception of the two samples from the active rivers (99C9 and 99C13), the grain size of those samples which were degassed by stepwise heating was reduced by two different procedures before analysis in order to diminish the proportion of noble gases from fluid inclusions [22]. Samples 99C8 and 99C12 were ground under pure ethanol in a polished agate mortar and then sieved in ethanol in order to obtain a grain size <100 μm. The other samples were ground in an agate mill for 20 min, which resulted in a grain size of <50 μm. Samples were then washed in acetone, dried, wrapped in Al or Ag foil and heated at $\sim$90°C overnight before being loaded into the sample carousel above the extraction furnace. Samples were degassed in four temperature steps at 400, 600, 800 and 1700 or 1750°C and the noble gases were analyzed in a VG5400 mass spectrometer. Blank values were nearly identical at extraction temperatures of 400, 600 and 800°C and on the order of 1×10^{-12} cm^3 ^{20}Ne, 0.05×10^{-8} cm^3 ^{40}Ar and 0.1×10^{-12} cm^3 ^{132}Xe. Blanks at 1700 or 1750°C were higher, with approximately 1.5×10^{-12} cm^3 ^{20}Ne, 0.5×10^{-8} cm^3 ^{40}Ar, and 0.2×10^{-12} cm^3 ^{132}Xe. We note that we cannot quantify the amount of Ne released from samples 00C10, 00C13, 00C11A, 00C11B and 00C11C in the highest temperature step, since in that sample series very high He and Ne blanks originating in the Mo liner of the furnace prevented a reliable determination. Fortunately, the blank problem did not occur at temperatures $\leq$800°C, where Ne_c is quantitatively released from quartz [4]. Blanks for mechanical crushing in vacuum are approximately 0.5×10^{-12} cm^3 ^{20}Ne, 0.05×10^{-8} cm^3 ^{40}Ar and 0.01×10^{-12} cm^3 ^{132}Xe.

He, Ne and Ar isotopes were determined in all temperature steps and by mechanical crushing. In some samples, Xe isotopes were determined in the 800 and 1700°C steps only. The abundances of ^{20}Ne, ^{40}Ar and ^{132}Xe, and the Ne, Ar and Xe isotopic compositions relevant for this study are compiled in Table 1. The complete noble gas data set, including He, ^{38}Ar, ^{84}Kr and all Xe isotopic ratios except ^{124}Xe/^{132}Xe and ^{126}Xe/^{132}Xe is available in the **Background Data Set**[1] (tables A1 and A2). All data have been corrected for analytical blanks, isobaric interferences and mass discrimination effects. Error limits correspond to the 95% confidence level; they include statistical uncertainties of the measurement, uncertainties of sensitivity and mass discrimination determination, and blank and interference corrections. Further information about the extraction line, interference corrections and technical details of the mass spectrometer can be found in Niedermann et al. [23].

Aliquots of seven quartz samples were analyzed for ^{10}Be and four of those samples were also analyzed for ^{26}Al using accelerator mass spectrometry (AMS) at the PSI/ETH facility in Zurich. Sample weights were of the order of 20–35 g. The chemical separation of Be and Al followed the procedure described in Ivy-Ochs [24], whereas the details of the AMS measurements are given in Kubik et al. [25]. Total Al contents were measured on aliquots of the dissolved quartz using ICP-AES with three standard additions per sample.

5. Results of noble gas analyses

The noble gas analyses of the amalgamated quartz samples, as summarized in Table 1, reveal the following systematic trends. With increasing temperature the ^{40}Ar/^{36}Ar ratio strongly increases from values between 300 and 600 at 400°C, i.e. slightly higher than the atmospheric ratio of 295.5, up to ^{40}Ar/^{36}Ar ratios of 2000–6000 at 1700°C (Fig. 3a). By far the largest fraction of ^{40}Ar is released at 1700°C (Fig. 3b). The ^{40}Ar/^{36}Ar ratio of the Ar component released by me-

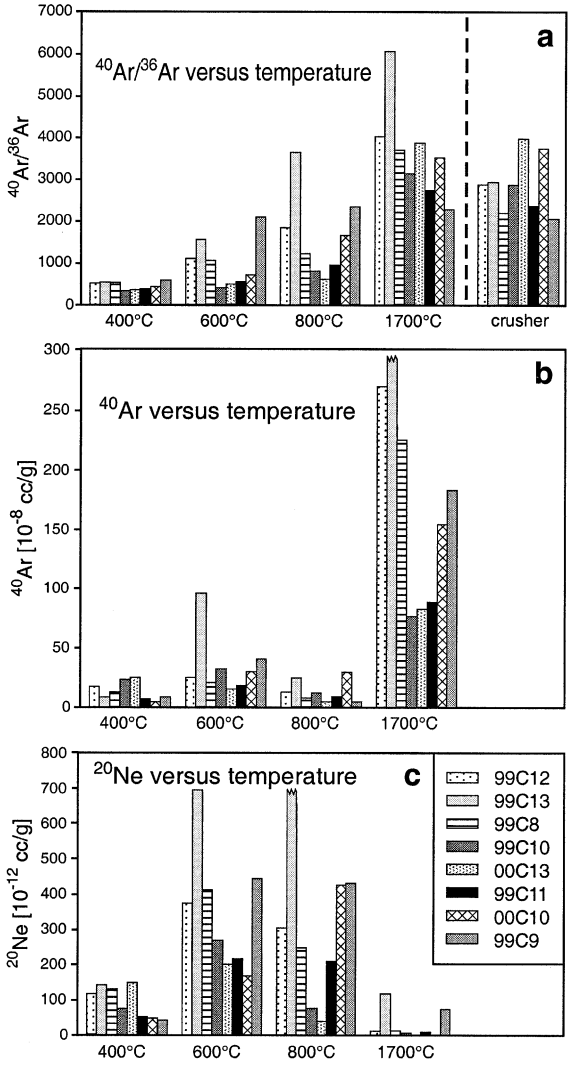

Fig. 3. Illustration of the Ar and Ne release characteristics of the investigated quartz samples, except for the subsurface samples (see Table 1). (a) $^{40}Ar/^{36}Ar$ ratios of the gas released at 400°C, 600°C, 800°C, 1700°C, and by crushing. (b) Amounts of ^{40}Ar released during the different heating steps. (c) Amounts of ^{20}Ne released during the different heating steps.

chanical crushing of the sample is either similar to that of Ar released at 1700°C or lies between the ratios obtained for the 800 and 1700°C steps (Fig. 3a). This observation indicates that Ar released at high temperature is mainly derived from fluid inclusions, which is also supported by the observation that the total amount of ^{40}Ar released, although variable for different samples, generally decreases with decreasing grain size in different samples (Table 1). Thus, grinding of the samples before gas extraction has liberated a significant proportion of the ^{40}Ar from fluid inclusions and this confirms the presence of a trapped component with high $^{40}Ar/^{36}Ar$ ratios.

As for ^{40}Ar, the largest amount of ^{132}Xe is released in the highest temperature step. However, in contrast to the $^{40}Ar/^{36}Ar$ ratio, the $^{134}Xe/^{132}Xe$ and $^{136}Xe/^{132}Xe$ ratios in the different heating steps are similar and, within error limits, identical to the atmospheric ratios of 0.388 and 0.330, respectively. The only exceptions are the 1700°C steps of the two active river samples (99C13, 99C9), which were not ground before gas extraction. Mechanical crushing of the quartz samples released a gas component with $^{134}Xe/^{132}Xe$ and $^{136}Xe/^{132}Xe$ ratios of $\sim$0.41 and $\sim$0.36, respectively, i.e. higher than the atmospheric ratios. This observation supports the conclusion derived from the Ar data that the fluid inclusions, which are opened by crushing in the vacuum system, contain a non-atmospheric crustal component. However, in contrast to ^{40}Ar the total amounts of Xe released during stepwise heating of the different samples increase with decreasing grain size. This implies that the grain size reduction and the increase in surface area due to grinding of the quartz lead to 'irreversible adsorption' of significant amounts of Xe from the atmosphere [26,27]. The adsorbed atmospheric Xe is released during stepwise heating and results in $^{134}Xe/^{132}Xe$ and $^{136}Xe/^{132}Xe$ ratios that are atmospheric within limits of error, i.e. the ratios do not show an increase towards the value released by crushing, except for the two river samples that were not ground but had the original grain size of $\sim$250–500 μm.

In contrast to Ar and Xe, the largest amounts of ^{20}Ne are released in the 600 and 800°C temperature steps, while the contribution of the 1700°C step is small (Fig. 3c). As noted above, we were not able to determine the amount of Ne in the 1700°C step of one sample series. However, samples with a grain size of $<$100 μm (99C12, 99C8)

or <50 μm (99C10, 99C11) that were analyzed earlier showed that only 1–2% of the total ^{20}Ne was released in the 1700°C step. We expect that similarly low ^{20}Ne amounts were released from the samples of the last series. In the 400°C step, the ^{21}Ne/^{20}Ne ratio of all terrace samples is considerably higher than the atmospheric value of 0.002959 (Table 1). At 600 and 800°C, the ^{21}Ne/^{20}Ne ratio decreases in all samples, except for 99C13, and approaches the value obtained by crushing. The elevated ^{21}Ne/^{20}Ne ratios suggest the presence of a cosmogenic Ne component that is indeed released at relatively low temperatures of $\leq$800°C [4]. The ^{21}Ne/^{20}Ne ratio of the component released by crushing is variable and ranges from 0.002993 (00C11C), a value close to the atmospheric ratio, up to 0.003975 (99C10). The Ne isotope ratios for the 400–800°C heating steps of all samples generally plot on or close to the spallation line as shown by Ne three-isotope diagrams of four representative samples (Fig. 4). The same is true for the Ne component released during mechanical crushing.

The degassing pattern of He is similar to that of Ne, showing concentration maxima in the 600 and 800°C steps and changing from a cosmogenic isotopic composition at low temperatures to a distinctly radiogenic one in the 800 and 1700°C steps (table A1 of the **Background Data Set**[1]). However, the He released by crushing is clearly dominated by the cosmogenic component, with ^{3}He/^{4}He ratios up to $\sim 10^{-4}$. A loss of cosmogenic ^{3}He from quartz by vacuum crushing has earlier been reported in [28] and is probably related to the poor retention properties of quartz for cosmogenic He [28,29]. Indeed, the total ^{3}He concentrations in our quartz samples are typically less than 10% of the ^{21}Ne$_c$ concentrations, although a production ratio $(^{3}\mathrm{He}/^{21}\mathrm{Ne})_c \sim 5$ would be expected. Therefore, since diffusional loss from quartz is so obvious, it is not surprising that part of the ^{3}He$_c$ does not find its way out of the crystal but diffuses into fluid inclusions, where it accumulates. A similar behavior for Ne is not expected because, unlike He, cosmogenic Ne is quantitatively retained in quartz under typical conditions of surface exposure, as indicated by the agreement of ^{10}Be and ^{21}Ne exposure ages [7,9].

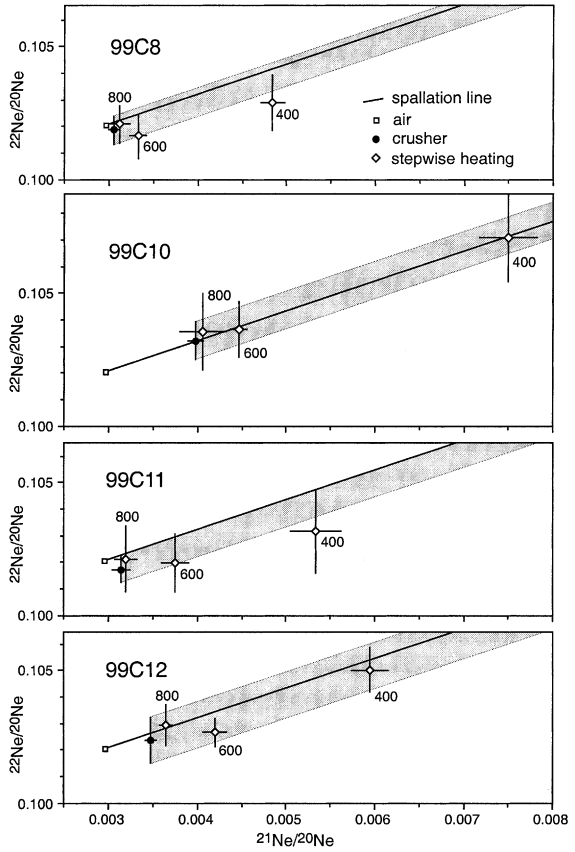

Fig. 4. Ne three-isotope diagrams for four samples showing the Ne isotope ratios of the component released by mechanical crushing and in the 400, 600 and 800°C heating steps. The gray field represents mixtures between a crustal Ne component, as revealed by crushing, and the cosmogenic Ne component.

6. Determination of surface exposure ages

6.1. The amount of cosmic ray-produced ^{21}Ne

For the calculation of a ^{21}Ne exposure age the amount of ^{21}Ne$_c$ must be determined and separated from other Ne components present in a sample. Commonly, the amount of ^{21}Ne$_c$ is quantified using the assumption that it is equal to the ^{21}Ne excess relative to a trapped component of atmospheric composition, i.e. $^{21}\mathrm{Ne}_c = [(^{21}\mathrm{Ne}/^{20}\mathrm{Ne})_{sample} - (^{21}\mathrm{Ne}/^{20}\mathrm{Ne})_{air}] \times {}^{20}\mathrm{Ne}_{sample}$. However, the Ne data from the analyzed quartz samples (Table 1, Fig. 4) unequivocally demonstrate that

the trapped Ne component released by crushing is not atmospheric but variable in composition. Although in some samples the Ne_{tr} component has a $^{21}Ne/^{20}Ne$ ratio similar to air, many samples have significantly higher $(^{21}Ne/^{20}Ne)_{tr}$ ratios. In consequence, the amount of $^{21}Ne_c$ must be quantified relative to the Ne_{tr} component with $^{21}Ne/^{20}Ne$ ratios varying between 0.002993 and 0.003975 for the different samples, i.e. $^{21}Ne_c = [(^{21}Ne/^{20}Ne)_{sample} - (^{21}Ne/^{20}Ne)_{tr}] \times {}^{20}Ne_{sample}$. For all samples the amount of $^{21}Ne_c$ is therefore smaller than the ^{21}Ne excess relative to air. To illustrate the significant difference between the two procedures, we show both values for the 400, 600 and 800°C heating steps and the total of these steps (Table 1). The largest difference is obtained for sample 99C10, which has a ^{21}Ne excess relative to air of 22.0×10^6 atoms/g, while the $^{21}Ne_c$ is only 10.7×10^6 atoms/g.

6.2. Correction for the inherited cosmogenic nuclide component

Before exposure ages can be derived, it is necessary to constrain the inherited cosmogenic nuclide content and subtract it from the total amount of $^{21}Ne_c$. The inherited component is constrained by two samples from active river channels and three subsurface samples from terrace T_1 at site 2. In order to tightly constrain the inherited cosmogenic nuclide component, we have not only analyzed Ne, but have also determined ^{10}Be and ^{26}Al concentrations of some samples. As the active river channels at the two study sites have catchment areas that differ in size and altitude, it is not surprising that the inherited component for the sites is different. Therefore, we discuss the data for the two sites separately.

6.2.1. Site 1

The sample from the active river channel of the Baiyang He near site 1 (99C13) has a ^{21}Ne excess of $4.6 \pm 2.8 \times 10^6$ atoms/g, as determined relative to the trapped component (Table 1). The large error limits result from the small differences between the $^{21}Ne/^{20}Ne$ ratios of the different heating steps and the $^{21}Ne/^{20}Ne$ ratio obtained by crushing. In order to estimate the inheritance of this sample more accurately, we have determined its ^{10}Be and ^{26}Al concentrations at $0.70 \pm 0.11 \times 10^6$ atoms/g and $4.28 \pm 0.66 \times 10^6$ atoms/g, respectively. We have converted these values into ^{21}Ne concentrations using $^{21}Ne/^{10}Be$ and $^{21}Ne/^{26}Al$ production rate ratios of 3.51 ± 0.74 and 0.54 ± 0.12 (see Section 6.3 for details) and obtain $2.46 \pm 0.62 \times 10^6$ and $2.30 \pm 0.61 \times 10^6$ atoms/g. Both values are in excellent agreement and in the lower range of the measured ^{21}Ne concentration of $4.6 \pm 2.8 \times 10^6$ atoms/g. To be consistent with site 2, where we have no ^{26}Al determination, we use only the ^{10}Be value as a constraint for the inheritance. Taking into account both values by calculating a mean would give an almost identical result. Since the inheritance in samples from active rivers is not necessarily an accurate measure of the inheritance of the older terrace deposits we double the error of the ^{10}Be concentration and use a conservative value of $0.7 \pm 0.2 \times 10^6$ atoms/g ^{10}Be for the inheritance correction of the terrace sample at site 1. This value is transformed to ^{21}Ne and ^{26}Al concentrations with the respective production rate ratios (see Section 6.3).

6.2.2. Site 2

The inherited cosmogenic nuclide component at site 2 is constrained by one sample from an active river channel (99C9) and three subsurface samples from terrace T_1. The river sample has a $^{21}Ne_c$ concentration of $1.4(+2.0/-1.2) \times 10^6$ atoms/g. The subsurface samples from depths of 0.6–0.65 and 1.2–1.25 m show decreasing $^{21}Ne_c$ concentrations with increasing depth, whereas the lowermost sample from 1.8–1.85 m has a slightly higher concentration than the intermediate sample (Fig. 5), without taking into account the relatively large error limits. To better constrain the cosmogenic nuclide content in the lowermost sample we use its ^{10}Be concentration of $0.511 \pm 0.052 \times 10^6$ atoms/g. This ^{10}Be concentration is the sum of the inherited component and a cosmogenic component that has been produced in situ at a depth of 1.8 m on terrace T_1. The ^{10}Be production rate at depth can be quantified by separately taking into account the depth dependency of nucleons [30] and muons [31] and assuming a density of 2.2–2.5 g/cm^3 for the sediments. At the surface,

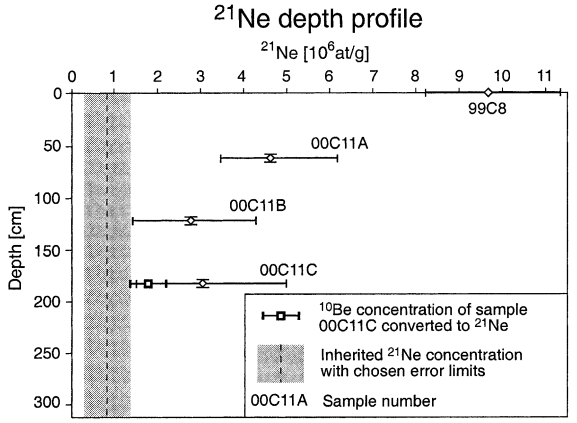

Fig. 5. Concentrations of $^{21}Ne_c$ in the surface sample (99C8) and three subsurface samples (00C11A, 00C11B, and 00C11C) from terrace T_1, plotted against depth. The ^{10}Be concentration of 00C11C, which has been converted to ^{21}Ne using the production rate ratio of 3.51 ± 0.74 (see Section 6.3), is also plotted. The decreasing concentrations of $^{21}Ne_c$ are consistent with the absence of post-depositional displacement of the clasts. The vertical dashed line indicates the value for the ^{21}Ne inheritance, derived from the ^{10}Be concentrations of the subsurface sample 00C11C and the active river sample 99C9. The gray field indicates the error limits chosen for the inheritance. For further explanation see Section 6.2.

the fraction of cosmogenic ^{10}Be produced by muons is around 2% at sea level [31] but only ~1% at 2000 m altitude. At 1.8 m depth and depending on the correct density, that fraction increases to ~4–8%. Within our level of accuracy, this is still of minor importance to the total production at 1.8 m depth, which turns out to be 5–10% of the surface value. As the surface sample from this terrace (99C8) has a ^{10}Be concentration of 3.0×10^6 atoms/g (Table 2), 5–10% of this value corresponds to $0.15–0.30 \times 10^6$ atoms/g. Reducing the ^{10}Be concentration of the subsurface sample at ~1.8 m depth (00C11C) by these values gives a range of $0.21–0.36 \times 10^6$ atoms/g ^{10}Be for the inherited cosmogenic nuclide content of sample 00C11C. This value is in excellent agreement with the active river sample (99C9), which has a ^{10}Be concentration of $0.256 \pm 0.038 \times 10^6$ atoms/g. This indicates that the inheritance derived from the active river sample provides a good approximation for the inheritance of terrace T_1. Nevertheless, the amount of the inherited nuclide component may have varied in the past. Therefore, we use a conservative value of $0.25 \pm 0.15 \times 10^6$ atoms/g ^{10}Be for the inheritance correction of the terrace samples from site 2 (Fig. 5) and convert this value to ^{21}Ne and ^{26}Al, again using the production rate ratios mentioned in the following section.

6.3. Production rates and surface exposure ages

The production rates of the different cosmogenic nuclides vary with latitude and elevation (e.g. [32,33]). To calculate surface exposure ages from measured nuclide concentrations corrected for inheritance, it is thus necessary to scale the production rates to the sampling locations. Both study sites at the Yumen thrust are located at latitude 39°51′N, however, at slightly different elevations; site 1 is at an elevation of 2000 m, whereas the mean elevation of the terraces at site 2 is 2030 m. To scale production rates published for sea level and high latitudes ($>60°$), we have applied the scaling method of Dunai [33]. We used the revised ^{21}Ne production rate of 19.0 ± 3.7 atoms/(g a) of Niedermann [34] and the production rates for ^{10}Be and ^{26}Al from Kubik et al. [25]. Since Kubik et al. [25] have applied the scaling method of Lal [32] to convert their measured concentrations to sea level and high latitude, we have first converted their original data with the method of Dunai [33] to sea level and high latitude and obtained production rates for ^{10}Be and ^{26}Al of 5.42 ± 0.46 and 35.3 ± 3.6 atoms/(g a), respectively (all errors have been converted to the 2σ level). These rates were then scaled to both study sites. We did not make any corrections for a temporal variation of the production rates, as Masarik et al. [35] expect that time-integrated production rates at latitude 40°N deviate less than 2% from the present-day values. The resulting production rate ratios of 3.51 ± 0.74 for $^{21}Ne/^{10}Be$ and 0.54 ± 0.12 for $^{21}Ne/^{26}Al$ have been used in the two preceding subsections for converting ^{10}Be and ^{26}Al concentrations into ^{21}Ne concentrations. Due to the small erosional denudation of the sampled areas on the pristine parts of the terraces, erosion is considered to have a negligible effect, as production rates of cosmogenic nuclides are approximately constant in the upper few centimeters

[30]. Therefore, the ^{21}Ne, ^{10}Be and ^{26}Al exposure ages summarized in Table 2 were calculated assuming no erosion. The error limits of the exposure ages reported in Table 2 do not include the uncertainties of the production rates and the scaling method.

7. Discussion

The quality of surface exposure ages determined for single geomorphic features is often difficult to assess due to the lack of independent geological arguments that constrain the age. Investigating a series of river terraces has the advantage that the relative age of the terraces is unequivocally determined, i.e. higher terraces are older than lower terraces. Evaluation of the ^{21}Ne surface exposure ages reveals that the ages are consistent with the relative age sequence of the terraces, as given by their height above active river channels (Table 2). The highest terrace located at site 1 has a ^{21}Ne age of 164 ± 26 ka, the lowest terrace at site 2 an age of 41(+17/−15) ka. Although the ^{21}Ne age for terrace T_1 (101+20/−18 ka) is slightly lower than that for terrace T_{2a} (112 ± 16 ka), the error limits of the two ages still allow T_1 to be older than T_{2a}.

Table 2
^{21}Ne, ^{10}Be and ^{26}Al surface exposure ages of terraces at Yumen thrust, Qilian Shan, China

^{21}Ne ages Sample locality	Sample ID	Height (m)	^{21}Ne ($\times 10^6$ atoms/g)	Error	^{21}Ne[a] ($\times 10^6$ atoms/g)	Error	Age (ka)	Error
Site 1: terrace	99C12	57	16.5	±2.0	14.0	±2.2	164	±25
Site 2: T_1	99C8	43	9.8	+1.7/−1.5	8.8	+1.7/−1.6	101	+20/−18
Site 2: T_{2a}	99C10	38	10.7	±1.3	9.8	±1.4	112	±16
Site 2: T_{2b}	00C13	35	7.20	+0.90/−0.69	6.3	+1.1/−0.9	72	+12/−10
Site 2: T_3	99C11	21	6.9	+1.5/−1.2	6.1	+1.6/−1.3	69	+18/−15
Site 2: T_4	00C10	18	4.5	+1.4/−1.2	3.6	+1.5/−1.3	41	+17/−15
^{10}Be ages Sample locality	Sample ID	Height (m)	^{10}Be[b] ($\times 10^6$ atoms/g)	Error	^{10}Be[a] ($\times 10^6$ atoms/g)	Error	Age[c] (ka)	Error
Site 1: terrace	99C12	57	4.66	±0.6	3.96	±0.63	168	±28
Site 1: active river	99C13	–	0.70	±0.11	–	–	–	–
Site 2: T_1	99C8	43	3.05	±0.46	2.80	±0.48	115	±20
Site 2: T_{2a}	99C10	38	3.34	±0.38	3.09	±0.41	127	±17
Site 2: T_3	99C11	21	2.35	±0.17	2.10	±0.23	85.9	±9.4
Site 2: active river	99C9	–	0.256	±0.038	–	–	–	–
Site 2: T_1, 1.8 m depth	00C11C	–	0.511	±0.052	–	–	–	–
^{26}Al ages Sample locality	Sample ID	Height (m)	^{26}Al[b] ($\times 10^6$ atoms/g)	Error	^{26}Al[a] ($\times 10^6$ atoms/g)	Error	Age[c] (ka)	Error
Site 1: terrace	99C12	57	29.4	±3.9	24.8	±4.1	169	±31
Site 1: active river	99C13	–	4.28	±0.63	–	–	–	–
Site 2: T_1	99C8	43	19.3	±2.8	17.6	±3.0	114	±21
Site 2: T_3	99C11	21	14.6	±1.8	13.0	±2.1	83	±14

Errors of ages (2σ) do not include uncertainties of production rates.

[a] Corrected for geological inheritance using the following values ($\times 10^6$ atoms/g):
Site 1: ^{21}Ne = 2.45 ± 0.87, ^{10}Be = 0.7 ± 0.2, ^{26}Al = 4.6 ± 1.4.
Site 2: ^{21}Ne = 0.88 ± 0.56, ^{10}Be = 0.25 ± 0.15, ^{26}Al = 1.6 ± 1.0.
^{10}Be values were transformed to ^{21}Ne and ^{26}Al using ^{21}Ne/^{10}Be and ^{26}Al/^{10}Be production rate ratios (see text for detailed explanations).

[b] Corrected for analytical blank.

[c] Corrected for radioactive decay of ^{10}Be and ^{26}Al.

The correction for the inherited component has a significant effect on the calculated ages. Neglecting the inheritance would raise the age of the terrace at site 1 by ~29 ka and the terrace ages at site 2 by ~10 ka, i.e. the geological blank at site 1 is about three times higher than that at site 2. This can readily be explained by the different characteristics of the catchment areas. We argue that the different geological blanks are mainly caused by the higher mean elevation of the Baiyang He catchment, as the production rates of cosmogenic nuclides increase approximately exponentially with altitude. The different sizes of the catchments and the resulting differences in the transport time of the clasts should only play a minor role, as suggested by a study of amalgamated quartz sand samples taken along a number of European rivers, which did not show substantial downstream increases of ^{10}Be concentrations [36]. A few previous studies have shown that the inherited component may be smaller than in the terrace deposits at the Yumen thrust. At the southern Tien Shan mountain front, individual cobbles from active streams with a diameter of 5–10 cm had an inherited component corresponding to an exposure age of only ~1–4 ka [20]. A study of terraces at the Kunlun fault in northern Tibet revealed that some cobbles on the lowermost terrace had very low ^{10}Be concentrations equivalent to only a few hundred years of surface exposure [37]. These cobbles were interpreted to reflect a recent flood event and place an upper limit on the inherited nuclide component [37]. On the other hand, amalgamated subsurface samples from river terraces in the U.S. revealed a variable inheritance equivalent to exposure ages of 10–40 ka [18,19]. Thus, while inheritance may be highly variable in different geomorphic settings, it should always be evaluated from active river and/or subsurface samples.

The ^{21}Ne surface exposure ages for the Yumen terraces have been calculated from the amount of excess ^{21}Ne relative to the crustal Ne component trapped in fluid inclusions. If the non-atmospheric ^{21}Ne/^{20}Ne ratio of the trapped component had not been identified and the ^{21}Ne excess relative to an atmospheric composition had been used for age analysis (see Table 1), the ^{21}Ne ages would be inconsistent with the relative age sequence of the terraces. At site 2, terrace T_{2a} would be about twice as old as T_1 and all other terrace ages would be too high. Furthermore, the age of 164 ± 26 ka obtained for the highest terrace at site 1 would be overestimated at ~300 ka. Combining the elevations of the terraces with their ages yields a vertical slip rate of 0.3–0.4 mm/a for the Yumen thrust fault (see [15] for a detailed tectonic and geomorphological interpretation of the exposure ages).

It has become clear that accurate ^{21}Ne exposure ages rely on a correct separation of cosmogenic ^{21}Ne from the trapped non-cosmogenic Ne component. A further test to demonstrate if the amount of cosmogenic ^{21}Ne has been reliably determined is an independent age estimate for the terraces using cosmogenic nuclides that do not have the inherent problem of non-cosmogenic components. Such nuclides are the radionuclides ^{10}Be and ^{26}Al, for which a significant accumulation of non-cosmogenic components over geological time scales can be ruled out due to their radioactive decay, which allows the non-cosmogenic fraction to reach only extremely low saturation levels. The fact that the ^{21}Ne exposure ages agree within error limits with the ^{10}Be and ^{26}Al ages demonstrates that the cosmic ray-produced ^{21}Ne component has been successfully separated from the trapped Ne component. The ^{10}Be and ^{26}Al determinations from the subsurface and the active river samples are also essential to accurately constrain the inherited cosmogenic nuclide component.

Significant amounts of non-atmospheric Ne trapped in fluid inclusions may be present not only in minerals precipitated in fractures, for instance quartz veins as documented in this study, but also in other rock types such as sandstones and different kinds of deformed metamorphic rocks. With respect to the latter it is noteworthy that ductile deformation in deep-crustal rocks is commonly associated with and may be triggered by fluids. Therefore, we expect that non-atmospheric Ne components trapped in fluid inclusions may be the rule rather than the exception. Groundwaters from the Canadian Precambrian shield, for example, have ^{21}Ne/^{20}Ne ratios ranging

from 0.00298 to 0.00848 [38], while natural gas samples from reservoirs in sedimentary basins have ratios up to 0.01 [39]. Surface exposure studies aiming to date relatively young geomorphic features with ^{21}Ne should take these observations into account by analyzing Ne isotopes deliberated by careful mechanical crushing. We are currently investigating the noble gas inventory of fluid inclusions in quartz from sandstones and will extend our studies to deformed metamorphic rocks in the near future.

Slightly elevated ^{134}Xe/^{132}Xe and ^{136}Xe/^{132}Xe ratios relative to air in the trapped component of the quartz samples might be taken to indicate the presence of U in the quartz samples from which ^{134}Xe and ^{136}Xe could have been produced by spontaneous fission. Thus, radioactive decay of U or Th might also have produced significant amounts of $^{21}Ne_n$ within the quartz crystals due to the reaction $^{18}O(\alpha,n)^{21}Ne$. The first obvious argument against the presence of nucleogenic ^{21}Ne are the ^{10}Be and ^{26}Al ages, which agree with the ^{21}Ne ages; if significant amounts of $^{21}Ne_n$ would be present, the ^{21}Ne ages would be higher than the ^{10}Be and ^{26}Al ages. In order to estimate the potential contributions of $^{21}Ne_n$, we have determined U concentrations in aliquots of four quartz samples. U concentrations as determined by thermal ionization mass spectrometry in the isotope laboratory of the GFZ Potsdam are 0.66 ppb in 99C12, 1.3 ppb in 99C8, 4.9 ppb in 99C10 and 1.3 ppb in 99C11. A first-order analysis using the following assumptions demonstrates that these very low U concentrations cannot produce significant amounts of $^{21}Ne_n$. First, we assign an age of 400 Ma to the quartz clasts, as they are presumably derived from quartz veins in the Paleozoic low-grade metamorphic sediments of the Qilian Shan that formed during a Devonian metamorphic event. This interpretation is supported by the low Al contents of the quartz samples (25–30 ppm), which indicate a relatively low formation temperature [40]. Second, we assume a U/Th ratio of one, which is a conservative assumption given that U is much more mobile than Th. Finally, we assume that the ratio of nucleogenic ^{21}Ne production to radiogenic ^{4}He production, i.e. α-particles, is 4.5×10^{-8} [41]. Using these assumptions, we calculate the contribution of nucleogenic ^{21}Ne generated by the $^{18}O(\alpha,n)^{21}Ne$ reaction to the total amount of $^{21}Ne_c$ as 0.3% in 99C12, 1.0% in 99C8, 3.4% in 99C10 and 1.4% in 99C11. This first-order calculation rules out a significant in situ production of nucleogenic ^{21}Ne in the quartz samples. As a consequence, we argue that the elevated ^{134}Xe/^{132}Xe and ^{136}Xe/^{132}Xe ratios are inherited from the crustal fluids that have been trapped in the quartz during their growth in veins at low-grade metamorphic conditions. The same interpretation is able to explain the high ^{40}Ar/^{36}Ar ratios of 2000–6000 of the trapped component, which result from radioactive decay of ^{40}K to ^{40}Ar in the crust and the enrichment of ^{40}Ar in the fluid phase that was present during the formation of the quartz veins. A similar interpretation was given in [13] to explain ^{40}Ar/^{36}Ar ratios of about 400–1000 measured in quartz from quartz–calcite veins present in lower greenschist-facies slates in the Apennines, Italy. The total amounts of ^{132}Xe, which are increasing with decreasing grain size, and the isotopic composition of Xe released during stepwise heating can only be reconciled by adsorption of considerable amounts of atmospheric Xe on the surface of the quartz crystals.

8. Conclusions

We have documented a crustal Ne component in quartz clasts that is non-atmospheric in composition and has been trapped in fluid inclusions during growth of the quartz crystals in veins at low-grade metamorphic conditions. We suggest that future ^{21}Ne exposure studies should evaluate the presence of trapped Ne components by mechanical crushing of the samples in vacuum. Only if the amount of cosmogenic ^{21}Ne is determined relative to this trapped Ne component can geologically meaningful ^{21}Ne exposure ages be derived. Prior to the age calculation, the inherited cosmogenic nuclide content, equivalent to ages of about 10–30 ka in our study, must be corrected for. This is most accurately achieved by analyzing active river and subsurface samples for ^{10}Be or ^{26}Al and converting the concentrations of these

radionuclides into ^{21}Ne concentrations. A significant in situ production of nucleogenic Ne in the quartz minerals is ruled out by extremely low U contents. Our results demonstrate the feasibility of ^{21}Ne surface exposure dating even under circumstances where a non-atmospheric trapped ^{21}Ne component is present. As the relative contributions of nucleogenic and trapped Ne components may vary considerably in different rock types, one of the future challenges in ^{21}Ne surface exposure dating is the quantification and reliable separation of these components from the cosmic ray-induced component, especially if young landforms are to be dated.

Acknowledgements

R.H. is indebted to Thomas Wiersberg, Tilmann Althaus and Enzio Schnabel for introducing him to the noble gas lab of the GFZ Potsdam and for many helpful discussions on all aspects of noble gas geochemistry and analysis. Thomas provided a number of Excel sheets that have greatly facilitated the evaluation of the noble gas analytical data. Rolf L. Romer is thanked for determining the U concentrations of four quartz samples. R.H. gratefully acknowledges invaluable logistic support from the Chinese Academy of Sciences in Lanzhou. We are grateful to Jörg Erzinger and Manfred Strecker for their support. Valuable and constructive comments by E. Brown and two anonymous reviewers are gratefully acknowledged. This project is financially supported by the Deutsche Forschungsgemeinschaft (DFG; Grant STR 373/10-1/2), the Chinese Academy of Science ('Knowledge and Creativeness Project') and the GeoForschungsZentrum Potsdam. *[BARD]*

References

[1] P. Sharma, R. Middleton, Radiogenic production of ^{10}Be and ^{26}Al in uranium and thorium ores: Implications for studying terrestrial samples containing low levels of ^{10}Be and ^{26}Al, Geochim. Cosmochim. Acta 53 (1989) 709–716.

[2] J.C. Libarkin, J. Quade, C.G. Chase, J. Poths, W. McIntosh, Measurement of ancient cosmogenic ^{21}Ne in quartz from the 28 Ma Fish Canyon Tuff, Colorado Chem. Geol. 186 (2002), 199–213.

[3] P. Eberhardt, O. Eugster, K. Marti, A redetermination of the isotopic composition of atmospheric neon, Z. Naturforsch. 20a (1965) 623–624.

[4] S. Niedermann, T. Graf, K. Marti, Mass spectrometric identification of cosmic-ray-produced neon in terrestrial rocks with multiple neon components, Earth Planet. Sci. Lett. 118 (1993) 65–73.

[5] B.M. Kennedy, H. Hiyagon, J.H. Reynolds, Crustal neon: a striking uniformity, Earth Planet. Sci. Lett. 98 (1990) 277–286.

[6] P. Sarda, T. Staudacher, C.J. Allègre, Neon isotopes in submarine basalts, Earth Planet. Sci. Lett. 91 (1988) 73–88.

[7] L.A. Bruno, H. Baur, T. Graf, C. Schlüchter, P. Signer, R. Wieler, Dating of Sirius Group tillites in the Antarctic Dry Valleys with cosmogenic ^{3}He and ^{21}Ne, Earth Planet. Sci. Lett. 147 (1997) 37–54.

[8] W.M. Phillips, E.V. McDonald, S.L. Reneau, J. Poths, Dating soils and alluvium with cosmogenic ^{21}Ne depth profiles: case studies from the Pajarito Plateau, New Mexico, USA, Earth Planet. Sci. Lett. 160 (1998) 209–223.

[9] J.M. Schäfer, S. Ivy-Ochs, R. Wieler, I. Leya, H. Baur, G.H. Denton, C. Schlüchter, Cosmogenic noble gas studies in the oldest landscape on earth: surface exposure ages of the Dry Valleys, Antarctica, Earth Planet. Sci. Lett. 167 (1999) 215–226.

[10] G.W. Wetherill, Variations in the isotopic abundance of neon and argon extracted from radioactive materials, Phys. Rev. 96 (1954) 679–683.

[11] J.F. Ziegler, Helium: Stopping Powers and Ranges in all Elemental Matter, Pergamon Press, Oxford, 1977, 367 pp.

[12] K.A. Farley, R.A. Wolf, L.T. Silver, The effects of long alpha-stopping distances on (U-Th)/He ages, Geochim. Cosmochim. Acta 60 (1996) 4223–4229.

[13] C.T. Harper, S. Schamel, Note on the isotopic composition of Ar in quartz veins, Earth Planet. Sci. Lett. 12 (1971) 129–133.

[14] T. Graf, C.P. Kohl, K. Marti, K. Nishiizumi, Cosmic-ray produced neon in Antarctic rocks, Geophys. Res. Lett. 18 (1991) 203–206.

[15] R. Hetzel, S. Niedermann, M. Tao, P.W. Kubik, S. Ivy-Ochs, B. Gao, M.R. Strecker, Low slip rates and long-term preservation of geomorphic features in Central Asia, Nature 417 (2002) 428–432.

[16] B. Meyer, P. Tapponnier, L. Bourjot, F. Métivier, Y. Gaudemer, G. Peltzer, G. Shunmin, C. Zhitai, Crustal thickening in Gansu-Qinghai, lithospheric mantle subduction, and oblique, strike-slip controlled growth of the Tibet plateau, Geophys. J. Int. 135 (1998) 1–47.

[17] R.S. Anderson, J.L. Repka, G.S. Dick, Explicit treatment of inheritance in dating depositional surfaces using in situ ^{10}Be and ^{26}Al, Geology 24 (1996) 47–51.

[18] J.L. Repka, R.S. Anderson, R.C. Finkel, Cosmogenic dating of fluvial terraces, Fremont River, Utah, Earth Planet. Sci. Lett. 152 (1997) 59–73.
[19] G.S. Hancock, R.S. Anderson, O.A. Chadwick, R.C. Finkel, Dating fluvial terraces with ^{10}Be and ^{26}Al profiles: application to the Wind River, Wyoming, Geomorphology 27 (1999) 41–60.
[20] E.T. Brown, D.L. Bourlès, B.C. Burchfiel, D. Qidong, L. Jun, P. Molnar, G.M. Raisbeck, F. Yiou, Estimation of slip rates in the southern Tien Shan using cosmic ray exposure dates of abandoned alluvial fans, Geol. Soc. Am. Bull. 110 (1998) 377–386.
[21] C.P. Kohl, K. Nishiizumi, Chemical isolation of quartz for measurement of in-situ-produced cosmogenic nuclides, Geochim. Cosmochim. Acta 56 (1992) 3583–3587.
[22] S. Niedermann, T. Graf, J.S. Kim, C.P. Kohl, K. Marti, K. Nishiizumi, Cosmic-ray-produced ^{21}Ne in terrestrial quartz: the neon inventory of Sierra Nevada quartz separates, Earth Planet. Sci. Lett. 125 (1994) 341–355.
[23] S. Niedermann, W. Bach, J. Erzinger, Noble gas evidence for a lower mantle component in MORBs from the southern East Pacific Rise: Decoupling of helium and neon isotope systematics, Geochim. Cosmochim. Acta 61 (1997) 2697–2715.
[24] S. Ivy-Ochs, The dating of rock surfaces using in-situ produced ^{10}Be, ^{26}Al, and ^{36}Cl, with examples from Antarctica and the Swiss Alps, Ph.D. dissertation no. 11763, ETH Zurich, Switzerland, 1996.
[25] P.W. Kubik, S. Ivy-Ochs, J. Masarik, M. Frank, C. Schlüchter, ^{10}Be and ^{26}Al production rates deduced from an instantaneous event within the dendro-calibration curve, the landslide of Köfels, Ötz Valley, Austria, Earth Planet. Sci. Lett. 161 (1998) 231–241.
[26] T.J. Bernatowicz, F.E. Kramer, F.A. Podosek, M. Honda, Adsorption and excess fission Xe: Adsorption of Xe on vacuum crushed minerals, J. Geophys. Res. 87 (Supplement) (1982) A465–A476.
[27] S. Niedermann, O. Eugster, Noble gases in lunar anorthositic rocks 60018 and 65315: Acquisition of terrestrial krypton and xenon indicating an irreversible adsorption process, Geochim. Cosmochim. Acta 56 (1992) 493–509.
[28] E.J. Brook, M.D. Kurz, Surface-exposure chronology using in situ cosmogenic ^{3}He in Antarctic quartz sandstone boulders, Quat. Res. 39 (1993) 1–10.
[29] T.E. Cerling, Dating geomorphologic surfaces using cosmogenic ^{3}He, Quat. Res. 33 (1990) 148–156.
[30] J. Masarik, R.C. Reedy, Terrestrial cosmogenic-nuclide production systematics calculated from numerical simulations, Earth Planet. Sci. Lett. 136 (1995) 381–395.
[31] E.T. Brown, D.L. Bourlès, F. Colin, G.M. Raisbeck, F. Yiou, S. Desgarceaux, Evidence for muon-induced production of ^{10}Be in near-surface rocks from the Congo, Geophys. Res. Lett. 22 (1995) 703–706.
[32] D. Lal, Cosmic ray labeling of erosion surfaces: in situ nuclide production rates and erosion models, Earth Planet. Sci. Lett. 104 (1991) 424–439.
[33] T.J. Dunai, Scaling factors for production rates of in situ produced cosmogenic nuclides: a critical reevaluation, Earth Planet. Sci. Lett. 176 (2000) 157–169.
[34] S. Niedermann, The ^{21}Ne production rate in quartz revisited, Earth Planet. Sci. Lett. 183 (2000) 361–364.
[35] J. Masarik, M. Frank, J.M. Schäfer, R. Wieler, Correction of in situ cosmogenic nuclide production rates for geomagnetic field intensity variations during the past 800,000 years, Geochim. Cosmochim. Acta 65 (2001) 2995–3003.
[36] M. Schaller, F. von Blanckenburg, N. Hovius, P.W. Kubik, Large-scale erosion rates from in situ-produced cosmogenic nuclides in European river sediments, Earth Planet. Sci. Lett. 188 (2001) 441–458.
[37] J. Van der Woerd, F.J. Ryerson, P. Tapponier, Y. Gaudemer, R. Finkel, A.S. Meriaux, M. Caffee, Z. Guoguang, H. Qunlu, Holocene left-slip rate determined by cosmogenic surface dating on the Xidatan segment of the Kunlun fault (Qinghai, China), Geology 26 (1998) 695–698.
[38] D.J. Bottomley, J.D. Ross, W.B. Clarke, Helium and neon isotope geochemistry of some ground waters from the Canadian Precambrian Shield, Geochim. Cosmochim. Acta 48 (1984) 1973–1985.
[39] H. Hiyagon, B.M. Kennedy, Noble gases in CH_4-rich gas fields, Alberta, Canada, Geochim. Cosmochim. Acta 56 (1992) 1569–1589.
[40] W.H. Dennen, W.H. Blackburn, A. Quesada, Aluminum in quartz as a geothermometer, Contr. Mineral. Petrol. 27 (1970) 332–342.
[41] I. Yatsevich, M. Honda, Production of nucleogenic neon in the earth from natural radioactive decay, J. Geophys. Res. 102 (1997) 10291–10298.